Available online at www.sciencedirect.com
ScienceDirect
Colloids and Surfaces A: Physicochem. Eng. Aspects 303 (2007) 14–29
COLLOIDS AND SURFACES A
www.elsevier.com/locate/colsurfa

Hydration and internal properties of polyelectrolyte multilayers

Monika Schönhoff [a,*], Vincent Ball [b], Andreas R. Bausch [c], Christophe Dejugnat [d], Nicolas Delorme [e], Karine Glinel [f], Regine v. Klitzing [g], Roland Steitz [h]

[a] *Institute of Physical Chemistry, University of Münster, Corrensstr. 30, D-48149 Münster, Germany*
[b] *Institut National de la Santé et de la Recherche Médicale,11 Rue Humann, Bâtiment 3, 67083 Strasbourg and Université Louis Pasteur, Faculté de Chirurgie Dentaire, 1 Place de l'Hôpital, 67000 Strasbourg, France*
[c] *Lehrstuhl für Biophysik-E22, Technische Universität München, Garching, Germany*
[d] *Institut de Chimie Séparative de Marcoule, 30207 Bagnols sur Cèze, France*
[e] *Max Planck Institute of Colloids and Interfaces, Am Mühlenberg, Potsdam, Germany*
[f] *Laboratoire Polymères, Biopolymères, Membranes – UMR 6522 CNRS – Université de Rouen, F-76821 Mont-Saint-Aignan, France*
[g] *Stranski-Laboratorium, Institut für Chemie, D-10623 Berlin, Germany*
[h] *Hahn-Meitner-Institut, Glienicker Str. 100, D-14109 Berlin, Germany*

Received 15 November 2006; received in revised form 23 February 2007; accepted 27 February 2007
Available online 3 March 2007

Abstract

In this review we summarize novel aspects of the hydration and internal properties of polyelectrolyte multilayers formed by layer-by-layer assembly. Reflectivity techniques monitor the water content and swelling behavior, while spin relaxation monitors water mobility. Odd–even effects in dependence on the number of layers are discussed in terms of an influence of the terminating layer. Other novel methodological approaches like X-ray microscopy or NMR cryoporometry address the water content in hollow capsules, and the water pore size distribution, respectively. Multilayer material properties are relevant for different applications. As a novel concept, dielectric properties are monitored in a field effect transistor device. Ion mobility and redox processes in multilayers are revealed by the electrochemical properties. Mechanical properties of multilayers, studied by colloidal probe atomic force microscopy depend on the conformation of the polymers involved.

Keywords: Polyelectrolyte; Multilayer; Layer-by-layer; Hydration

1. Introduction

Electrostatic interactions between polyelectrolytes and charged surfaces are the basis for building up multilayer materials of polyelectrolytes of alternating charge by layer-by-layer assembly [1]. The field of polyelectrolyte multilayers (PEM) has, after a tremendous increase of the number of publication already in the 1990s, even expanded further in the past years. A major development and trigger towards novel types of applications certainly was the development of hollow polymeric capsules. Capsules can be prepared by adsorbing polyelectrolyte multilayers on colloidal templates and subsequently removing the core [2,3]. Polyelectrolyte multilayers have numerous potential applications in various fields such as containers, sensors, drug delivery, etc. Past review articles have summarized the state of the art of multilayers and their properties [4–10], and of capsules with respect to release applications [11,12].

In the early years, structural parameters such as the layer thickness or surface coverage were the main tools to follow multilayer formation, where in particular X-ray and neutron reflectivity revealed aspects of layer growth and internal entanglements [13–15]. Today, an enhanced understanding of the internal properties of the multilayer assembly is developing. A major interest in these films is the possibility to tune the composition of the membrane and its thickness on the nanometer scale. Here, one of the most important question concerns the water content of the multilayer film or capsule wall, respectively, which determines key properties like permeability and elasticity.

* Corresponding author. Tel.: +49 2518323419; fax: +49 2518329138.
E-mail addresses: schoenho@uni-muenster.de (M. Schönhoff), vincent.Ball@medecine.u-strasbg.fr (V. Ball), abausch@ph.tum.de (A.R. Bausch), christophe.dejugnat@cea.fr (C. Dejugnat), nicolas.delorme@univ-lemans.fr (N. Delorme), karine.glinel@univ-rouen.fr (K. Glinel), klitzing@chem.tu-berlin.de (R.v. Klitzing), steitz@hmi.de (R. Steitz).

0927-7757/$ – see front matter © 2007 Elsevier B.V. All rights reserved.
doi:10.1016/j.colsurfa.2007.02.054

The hydration water controls the local molecular interactions, especially the polyion–polyion complexation. In addition, the relevance of hydrophobic interactions in layer formation is increasingly discussed [16].

In the first part of this article, we summarize recent studies of hydration of PEMs. Reflectivity studies can monitor the water content and swelling behavior. As a novel experimental approach, X-ray microscopy can extend analysis of the water content to capsule systems and add spatial resolution to the information. NMR techniques such as spin relaxation or cryoporometry are based on the dynamic properties of the hydration water in PEMs: spin relaxation gives information about the hydration water mobility, and cryoporometry monitors the pore size distributions in PEMs. Finally, an example of an approach to control the water content is given, where wax nanoparticles are employed.

In the second part of the article we describe investigations of different material properties of PEM which have major relevance for applications. The dielectric properties were monitored by a novel transistor-based approach, while the permeability of PEMs towards small multivalent ions is an important issue in separation applications. Finally, the mechanical properties are described by colloidal probe AFM experiments on flat PEM films.

2. Hydration of polyelectrolyte multilayers

2.1. Water content determined by reflectivity methods

Concerning structural investigations of PEM, which provide data on the water content, there were mainly scattering experiments involved, dealing with film thickness and polyelectrolyte density in multilayers at the solid/air interface. As the polyelectrolyte layers are very sensitive to the water content of the environment, it is necessary to conduct structural investigations also at the solid/liquid interface to clarify the internal structure in situ. A few years ago a direct cross-check of the film structure was performed employing X-rays at the solid/air and neutrons at the solid/liquid interface of the same films built from poly(styrene sulfonate)/poly(allylamine hydrochloride) (PSS/PAH) bilayer pairs [17]. This investigation revealed pronounced differences between the freshly adsorbed part (ad-part) and the re-swollen precursor part of the films at the solid/liquid interface. The analysis of the neutron reflectivity of the solvent swollen film prior and after adsorption of six additional (PSS/PAH) bilayers strongly suggested a significantly increased amount of water and thus an increased scattering length density of the ad-part of the multilayer. The water volume fraction of 42% found inside the precursor film after moderate swelling (∼10%) upon exchange of the environment compared well with the value reported for a very similar multilayer examined in saturated D_2O atmosphere [15]. The water volume fraction inside the freshly adsorbed ad-part was much higher. It was estimated to 56%. This part of the multilayer stack shrunk upon drying by 50%. The X-ray reflectivity patterns of this film taken at the solid/air interface, prior and after adsorption of the ad-part revealed no difference between precursor and ad-block in the "dry" state at ambient conditions. As mentioned above, the thickness of polyelectrolyte films is dependent on the amount of water sorbed from the environment [15,17]. Dehydration over P_2O_5 leads to shrinkage of films previously investigated in ambient laboratory atmosphere due to the evaporation of water from the multilayer structure. It is assumed that the polymer network tightens on dehydration without rearrangement of the loop structures within the layers with no lateral inhomogeneity being inferred in the dehydration process. This would mean that water molecules are removed from the polymer network and that they leave a void volume within the film, which is not completely filled by the polymer upon film shrinkage, presumably because of steric hindrance of the polymer chains. The polyelectrolyte multilayers were found to re-swell almost completely in saturated D_2O atmosphere. From the re-swelling experiments it was shown that the average water content inside fully hydrated films (100% relative humidity, r.h.) is larger than 40% by volume with twice as much water associated with PSS as with PAH [15]. This corresponds to eight water molecules associated with one ion pair in a polyanion/polycation complex. Farhat et al. [18] found a hydration number of 6 for the system PSS/PDADMAC (PDADMAC: poly(diallyl dimethylammonium chloride) by infrared spectroscopy. The difference was explained by a higher C/N^+ ratio, *i.e.* higher hydrophobicity, in the latter case. Those numbers are further corroborated by a very recent ATR-FTIR investigation on counterions and water uptake in polyelectrolyte multilayers as a function of salt doping. Jaber and Schlenoff found six water molecules associated with each PSS/PAH and seven water molecules associated with each PSS/PDADMAC pair [19]. Glinel et al. also found a D_2O content of about 50% in a completely swollen PSS/PAH multilayer [20]. Irrespective of the substrate and the presence of an initial PEI layer a maximum water content of about 75% was reported for PLL/PGA (PLL: poly-L-lysine; PGA: polyglutamic acid) multilayers prepared under physiological conditions [21].

The incorporation of inorganic particles into multilayers seems to reduce the water content. Multilayers of unilamellar titania crystallites and PDADMAC contain about 18 vol.% of water in a r.h. of 90% [22]. The titania film needed more than 1 h to be equilibrated with the surrounding moisture. Kleinfeld and Ferguson have reported a similar hydration/dehydration process for a multilayer film of laponite sheets and PDADMAC which takes place within seconds [23]. This difference in kinetics may be related to the chemical nature of the nanosheet crystallites. The Titania nanosheet has a higher charge density than smectite clay minerals which consequently leads to higher hydration energy.

Experiments done with ellipsometry showed that the steady-state value (thick multilayers) for water was much lower (20–25%) than in neutron reflectometry studies (40–55%). The experimental error was less than 10%. Hence, experimental impreciseness cannot be the reason. The principal difference between both methods is that in case of neutron reflectometry studies D_2O is used, while the present ellipsometry studies are carried out against H_2O. This gives a hint for an isotopic effect being observed. Since the thickness is more or less the same the density of D_2O must be higher than that of H_2O. One reason for

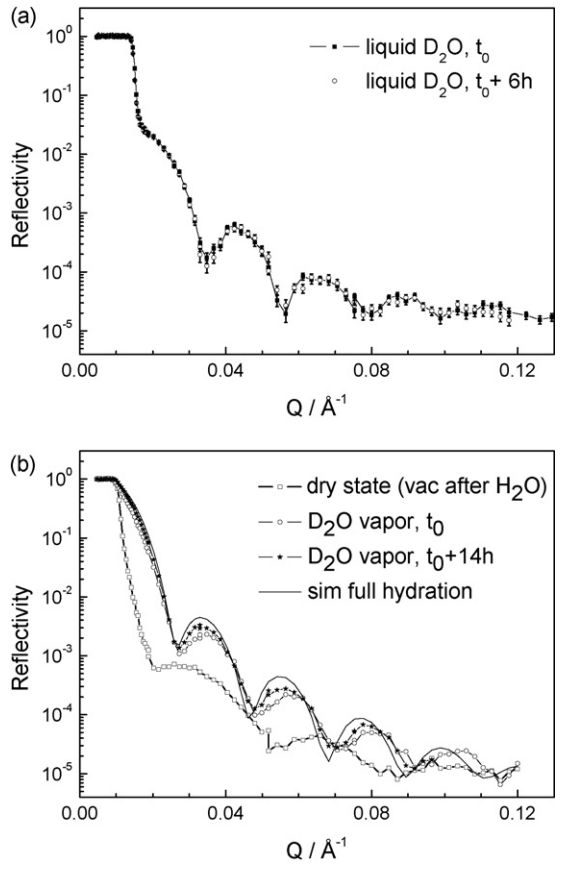

Fig. 1. Subsequent neutron reflectivity curves from a PSS/PAH multilayer against liquid D_2O (a), and against saturated D_2O vapor (b). While the reflectivity curves against liquid D_2O fully superimpose (with equilibration time in the minutes range), there is a strong time dependence of the measurements against D_2O vapor. Note, that the expected final state (sim full hydration), as calculated from the water content of the fully swollen film against liquid D_2O, is not reached even after 14 h exposure to D_2O vapor. Both multilayers were exposed to H_2O before drying and brought into contact to D_2O (liquid or vapor) then.

a different total amount of water could be the different ability to form hydrogen bonds [24,25].

Differences in the kinetics of water uptake and release are also observed between the exposure to saturated water vapor and to liquid water. Neutron reflectometry measurements on PSS/PAH or PSS/PDADMAC multilayers showed that swelling against liquid water was finished within the first minutes. Fig. 1a shows the coincidence of two sequential neutron spectra of polyelectrolyte multilayers against liquid water. This kinetics stays fast irrespective of the water isotope, and the water isotopes are exchanged instantaneously. If the multilayer was exposed to the same water isotope before and after drying, no time effect was detected, and also the water uptake from *vapor* was very fast (not shown here). The equilibrium water content after exposure to liquid water or vapor must be the same, since the chemical potential of saturated vapor and liquid water is the same. For instance, after storing a coated wafer in saturated water vapor the contact angle did not change anymore. This means that the deposition of the water droplet did not change the surface anymore, and the multilayer had been already completely swollen before the droplet was put on the surface The experimental difficulty is to ensure 100% r.h. Especially at high r.h. the multilayer is sensitive to small changes in r.h., *i.e.* for small derivations from saturated vapor [26]. In contrast to this, the water uptake against vapor may take several days [24,25] if the isotopes are exchanged. Starting from the dry state after preparation (*i.e.* after exposure to H_2O), and transferring the multilayer into D_2O vapor an equilibrium could be not detected even after days. Fig. 1b shows the spectra before and after exposure to D_2O vapor. The solid line indicates the reflectivity at full hydration, which is not reached within the experimental time. This leads to the conclusion, that the exchange of H_2O molecules by D_2O molecules takes much longer (order of days) than the water uptake itself (order of min).

2.2. Water content determined by soft X-ray microscopy

A novel approach to access the water content was recently developed by employing X-ray microscopy. This technique is particularly promising, because of its applicability to volume systems, *i.e.* hollow microcapsules: polyelectrolyte capsules are routinely characterized at the micrometer scale by confocal microscopy, which provides information about the global shape of capsules in water, and also by atomic force and electron microscopy that allow measurement of the membrane thickness and roughness at the nanometer scale. However, these later techniques cannot provide such high resolution information in environmental conditions – *e.g.* in aqueous suspension – because they require drying of the specimen.

Here, full-field transmission X-ray microscopy (TXM) developed at BESSY II (Berlin) was used [27], which allows the observation of soft matter in aqueous environment with a high resolution of 20 nm. In the so-called "water window" (E = 284–543 eV) a natural contrast is obtained. This "window" corresponds to photon energies between the K shell absorption edge of carbon and oxygen, where water molecules absorb less than carbon-rich substances. Temperature sensitive microcapsules, consisting of four double layers of PDADMAC and PSS, irreversibly shrink upon heating from 4.5 to 1.3 μm with a concomitant increase of the shell thickness [28]. TXM was used to investigate the morphological changes, as well as the variation of the wall composition of these polyelectrolyte capsules brought in under heating.

After imaging capsules heated at different temperatures (20, 50, 70, and 90 °C), transmission profiles were extracted along the diameters of the shells (Fig. 2). These curves were fitted using a simple model of a hollow sphere with a constant density in the membrane.

The calculations yielded geometrical parameters (such as size and membrane thickness) as well as density of the hydrated polyelectrolyte multilayers. This density is reduced compared to that of dry PDADMAC/PSS precipitate because of voids filled with water within the multilayer membrane. Comparing the apparent density to that of dry precipitate yielded the volume fraction and also the amount of hydration water. The results are presented in Fig. 3 and show a partial dehydration of the multilayers during the temperature-induced rearrangement.

Before heating the multilayers are highly hydrated (78% water). It is worth to note that the water content of the cap-

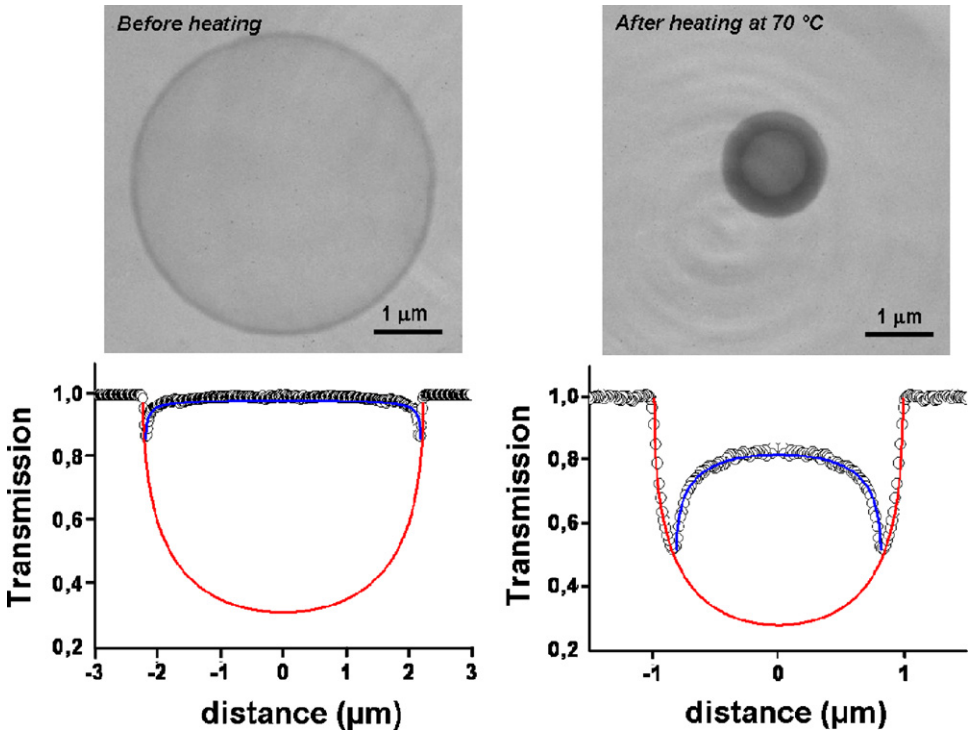

Fig. 2. TXM micrographs of initial $(PDADMAC/PSS)_4$ capsules and after heating for 20 min at 70 °C in water, and the corresponding fitted transmittance profiles.

sule walls is much higher than of the same material prepared on planar interfaces (45–55% water). This indicates a more loosely packed structure in case of capsule wall material. Moderate heating excluded about 10% of the water, while heating at 70 °C or more clearly produces a weakly hydrated "glass". The walls contain finally only about 45% of water after such a drastic shrinkage.

As a conclusion, direct quantitative imaging of soft matter in environmental conditions by soft X-ray microscopy is a very promising technique that opens new application for chemical physics. Making use of the different absorption coefficients of oxygen and carbon, material distribution and water content can be quantified by analysis of the transmission images. In the case of temperature sensitive PDADMAC/PSS microcapsules, this technique validated and quantified the transition of hollow shells to filled spheres upon heating above 70 °C. The water content remained low approaching room temperature, which was consistent with the glassy state of the system.

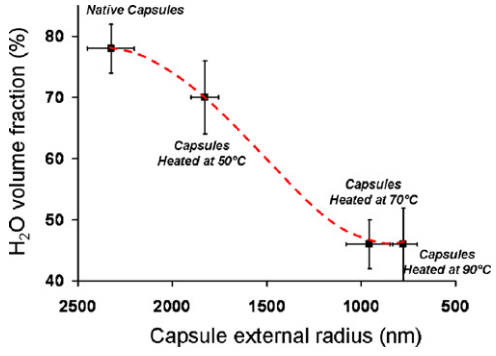

Fig. 3. Water content as a function of the external radius for capsules heated at different temperatures.

2.3. Odd–even effects in PEMs

Due to the alternating deposition of polycations and polyanions the surface potential of the outermost layer, terminating the assembly, commonly varies between positive and negative values. This causes alternating external conditions for the multilayers. For a number of multilayer properties, reversible variations with the sign of charge of the terminating layer were observed, which became evident as 'odd–even' effects in dependence on the number of single layers, n. Evidently, surface properties such as the ζ-potential are determined by the terminating layer, therefore ζ is reversibly alternating [3]. Similarly, water contact angles alternate, reflecting the surface energy of the terminating layer [26,29]. In contrast, the influence of the terminating layer on internal multilayer properties is not directly evident. The electrostatic potential, which decays into the multilayer assembly, changes sign in dependence on the sign of charge of the terminating layer. This can have an influence on the internal electrochemical properties and lead to an alternating odd–even behavior of averaged properties of multilayers in dependence on n.

For example, the average dissociation of carboxylic groups in multilayers was increased by a terminating polycation layer, and decreased by a terminating polyanion layer, as shown by IR spectroscopy [30]. For a weak polyelectrolyte layer of PMA embedded in a multilayer system of strong polyelectrolytes the degree of dissociation depended on the charge of the terminating

layer [31]. The second harmonic generation (SHG) efficiency alternated with the number of layers [32].

Very pronounced odd–even effects were found in the mobility of the hydration water in multilayers [33]. In this study, the method of solvent spin relaxation monitors the average mobility of the water in aqueous dispersions. This technique was applied to the hydration water during the process of adsorption of the polycation PAH to latex particles and to multilayers on particles, respectively [34]. While for adsorption to bare particles different mobilizing and immobilizing contributions to the net water mobility are found, the adsorption of PAH to multilayers was accompanied by a large decrease of the net water mobility [34]. Since the specific relaxation rate is proportional to the product of the bound fraction of water and the motional correlation time, this implies either a large increase of the bound fraction, or a reduction of the average water mobility. A study of the dependence on the number of layers could attribute the large water immobilization to a reversible odd–even effect, see Fig. 4 [33]. Upon adsorption of a PAH layer, the water mobility is decreasing, detected by an increase of the specific relaxation rate, R_{2sp}. R_{2sp} is proportional to the fraction of water bound in layers, f_B, and its motional correlation time, τ_C. Hence, an increase of R_{2sp} is either due to an increase of f_B, and thus a swelling of the layers, or an increase of τ_C, *i.e.* a reduction of the dynamics of the bound water. Upon adsorption of a PSS layer, the water mobility is increasing again, see Fig. 4. Interestingly, this odd–even effect was observed for PAH/PSS, but not for PSS/PDADMAC internal layers, where R_{2sp} was increasing monotonously with n [33].

However, employing PDADMAC as the terminating layer on a PAH/PSS multilayer system, the water mobility could again be controlled, see solid triangles in Fig. 4. It was thus concluded that the odd–even effect is not controlled by the hydration properties of the terminating layer itself, but that it is the sign of the surface potential which induces changes of the water mobility in the internal layers. In addition, as can bee seen from Fig. 4,

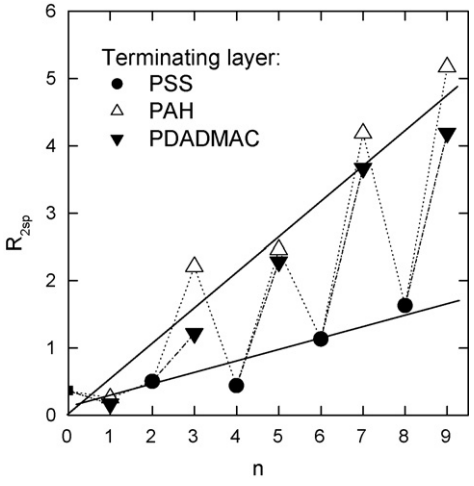

Fig. 4. Specific relaxation rate of water protons reflecting water immobilization in dispersions of colloids coated with n layers of PAH/PSS [33]. Dashed lines are connecting the data points. Full lines visualize the amplitude of the odd–even effect.

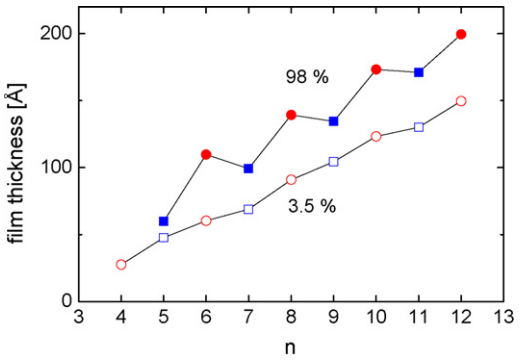

Fig. 5. Multilayer thickness in dependence on the number of deposited layers for two different relative humidities [26].

the amplitude of the odd–even effect is increasing linearly with the number of layers, which is further evidence of an integrated effect over all internal layers up to at least $n = 9$ [33]. It was concluded that reversible variations of the hydration water dynamics in PSS/PAH multilayers occur in dependence of the potential of the terminating layer. In addition, odd even variations of water mobility were also detected by measurements of the spin–spin relaxation rate R_1 [35,36].

It was speculated whether this odd–even effect in water mobility is associated with swelling and de-swelling, *i.e.* a variation of the water fraction f_B in the multilayer [33]. In order to distinguish between the influence of f_B or τ_C, respectively, structure sensitive methods like neutron reflectometry and ellipsometry were used to determine the water content. For this purpose, several studies dealt with multilayers at planar interfaces, employing identical preparation conditions as for multilayers on particles, *e.g.* no intermediate drying of the layers.

After drying of such layers, ellipsometric layer thickness data were measured for films in equilibrium with water vapors for two different humidities, see Fig. 5. While the thickness of a PSS/PAH multilayer after drying (at 3.5% r.h.) increases linearly with n, the thickness in the water swollen state depends on the outermost layer and increases in zigzag shape. After the deposition of PSS the film swells and PAH adsorption leads to shrinking. This was also obvious in the refractive index, which is larger for films containing less water, *i.e.* with PAH outside [26].

The decrease of thickness upon PAH adsorption indicated that water is pressed out of the multilayer when PAH is adsorbed, while again more water diffuses into the multilayer upon adsorption of the next PSS layer [26]. It is worth to mention that the zigzag shape of the upper curve in Fig. 5 is indeed due to swelling and de-swelling by water and has nothing to do with a loss in polymer material, as confirmed by the linear increase under dry conditions (3.5% r.h.).

These results could mean that PSS associates more water than PAH. Interpreting this in context with the above NMR data, it could be the swelling after PSS adsorption which remobilizes the water within the multilayer. Due to the swollen structure after the adsorption of PSS there could be ‘voids’ for mobile water. After the adsorption of a PAH layer, the multilayer structure is slightly more compressed, whereby part of the water

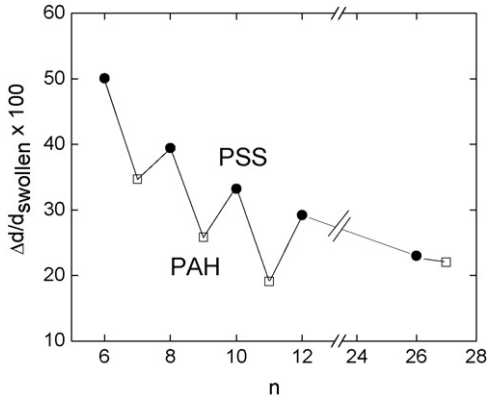

Fig. 6. Volume fraction of the exchangeable water in dependence of the number of adsorbed layers [26], expressed as the swelling ratio, where it is $\Delta d = d_{\text{swollen}} - d_{\text{dry}} = d$ (98% r.h.) $- d$ (3.5 r.h.).

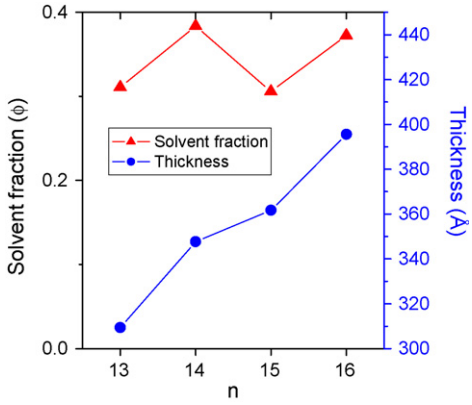

Fig. 7. Average solvent fraction and total layer thickness for multilayers of PAH/PSS prepared with 1 M NaCl. The even numbers of layers correspond to multilayers terminated with PSS [37].

can be expelled and part of the mobile water can be immobilized. Fig. 6 shows the relative change in thickness $\Delta d/d_{\text{swollen}}$ due to water uptake in saturated vapor in dependence on the type of polyelectrolyte in the terminating layer. This relative change in thickness is related to the exchangeable water and does not reflect the amount of water, that cannot be removed by simple drying (*e.g.* hydration water). The latter type of water does not show any odd–even effect, since the thickness at dry air (r.h. = 3.5%) increases monotonically in Fig. 5. However, the amplitude of thickness variations in saturated vapor is low compared to that of the variations in spin relaxation rate. Furthermore, the difference between the water content for a PAH surface and PSS surface decays rapidly with the number of layers, see Fig. 6. The average ratio of exchangeable water content levels off at 23% in a 26-layer film.

It is concluded that in terms of layer thickness, a few outer layers only respond to the deposition of the next polyelectrolyte layer, while the inner layers remain more or less unaffected. Thus, the small odd–even effect of the total water content becomes less pronounced with increasing number of layers.

A neutron reflectivity study was also performed at identical preparation conditions as for multilayers on colloids [37]. Here, structural data were taken in situ during the adsorption process, *i.e.* the layers were characterized in contact with water to ensure comparability with the layers of the NMR study. However, in order to allow an adequate data analysis, the minimum thickness of multilayers for neutron reflectometry experiments should be 200–300 Å (*i.e.* thicker than in ellipsometry experiments). Therefore, 27–30 layers were deposited at 0.25 mol/L NaCl. For these conditions odd–even variation was detected neither in total thickness, nor in solvent fraction. However, for layers prepared at 1 mol/L NaCl with a similar total thickness, an odd–even effect was detected in the solvent fraction; while the layer thickness showed a monotonous increase, see Fig. 7. This implies that in spite of a monotonous layer growth without swelling or de-swelling, internal properties of the hydration water, *i.e.* the density, can be driven by the outer potential, giving rise to variations of the solvent fraction. Multilayers with PSS as the terminating layer yield a larger solvent fraction than the ones with PAH outside, which is consistent with the trend in the ellipsometric thickness data taken against vapors.

The occurrence of odd–even variations in layer thickness can be discussed as dependent on the number of adsorbed layers, n. For small n ($n < 13$) an odd–even effect occurs with respect to the thickness and solvent fraction. With increasing n the amplitude of thickness variations becomes smaller, while the variation of the average water fraction is still apparent. At large n, $n > 25$, finally, both variations have decayed. This is consistent with previous studies which showed that a region of a few outer layers differs from the internal layers. For example, the outer layers contain a larger fraction of water, as shown above by the decrease in average water content in PSS/PAH multilayers with increasing n. The influence of the zone of loosely packed outer layers decreases with n for properties averaged over the whole multilayer. Similarly, for PLL/PGA multilayers, such a decrease of water fraction was observed for $n > 6$ [21]. A proof of an inhomogeneous density profile had also been given by permeability [38] and mobility studies [39].

Thus, the small odd–even variations observed in ellipsometry can be attributed to the properties of a few outer layers, which are subject to swelling and de-swelling in dependence on the terminating layer. With increasing number of layers, these variations are less pronounced, as internal layers dominate the film properties. Variations of the average solvent fraction decay less rapidly, as they are still pronounced for n around 15, but have decayed for n above 25.

As to the strongly pronounced odd–even variations in spin relaxation experiments, the following conclusions can be drawn. Variations in thickness or solvent fraction cannot be responsible for the odd–even effect of spin relaxation for two reasons. First, the amplitude of the water content (*i.e.* thickness and solvent fraction) never varies by more than 20%. Second, thickness variations are only present in a few outer layers and steeply decay already below $n < 10$. In contrast to this, the odd–even effect of the water mobility still increases with n in this regime, and the mobilization can change by more than a factor of 4 within the studied region of layer numbers. Thus, the dominating influence on $R_{2\text{sp}}$ is clearly due to odd–even variations of the motional correlation time. Hence, the odd–even variation has to

be attributed to a dependence of water dynamics on the sign of surface potential of the terminating layer.

The molecular mechanisms for these different aspects of odd–even variations are not finally clarified. Under the assumption that the change in surface potential controls both water content and water mobility, the decay length of the potential of the outer layer must be quite large (*i.e.* in the order of several tens of nanometers). In dissociation experiments, the decay length in multilayers was estimated to 10 layers [31], while in spin relaxation experiments no saturation of the odd–even amplitude was observed up to nine layers [33], which implies a decay length of at least 15 nm. Negligible counterion content in PEM and a low dielectric constant might cause a large internal Debye length. This would be in agreement with the long decay length reported in Section 3.1 and in [40], induced by a concentration of free ions in the order of 10^{-4} to 10^{-3} mol/L within the multilayer at moderate permittivity (ε_r: 20–50).

In conclusion, there are in the meantime a number of experiments demonstrating odd–even variations in PEM. The effect of the terminating layer on average multilayer properties is rather different. While effects on the total multilayer thickness related to swelling and de-swelling of water are little pronounced and occur only in a few outer layers, the influence on water mobility in multilayers is significantly more pronounced and has a larger decay length.

2.4. Pore size distributions in polyelectrolyte multilayers

A novel approach of determining pore sizes has recently been applied to polyelectrolyte multilayers [41]. In NMR cryoporometry, the multilayers are considered as a porous material, where any free volume, *i.e.* in voids, which is occupied by hydration water is interpreted as pores of different size. The Gibbs–Thompson equation describes the relation between the freezing point depression of a liquid and the size of a small spherical volume, which it is occupying. Samples consisting of concentrated dispersions of PEM-coated colloidal silica were cooled and upon subsequent heating the liquid water 1H signal was detected in dependence of temperature. Liquid water was detected at temperatures as low as −80 °C, demonstrating the presence of nanopores where water has a large freezing point depression. Fig. 8 shows the increase of the amount of liquid water with increasing temperature. Here, water in pores of increasing size is successively melting. A model assuming log–normal distributions of the motional correlation time of water allowed to fit different pore size modes to these curves [41]. For the colloidal silica employed as the template, two pore size modes were identified (dashed curve). For coated particles, the total water signal was dominated by water in a pore size mode arising from the multilayers, see dotted curve.

Pore size distributions were extracted from a quantitative analysis and decomposition of the different contributions. The pore size distribution in multilayers showed a maximum around 1 nm, and a width implying that pore sizes of up to 3 nm occur, see Fig. 9 [41].

A slight dependence of the average pore size on the number of layers, n, was found. The average sizes are 1.2, 1.3, 1.4, and 1.5 nm for $n = 7$, 8, 9, and 10, respectively [41]. Larger pores could be the consequence of a more loose packing of the polymer layers with increasing n, while in a multilayer system with small n, the pore size distribution is dominated by a close packing of the first layers on the substrate.

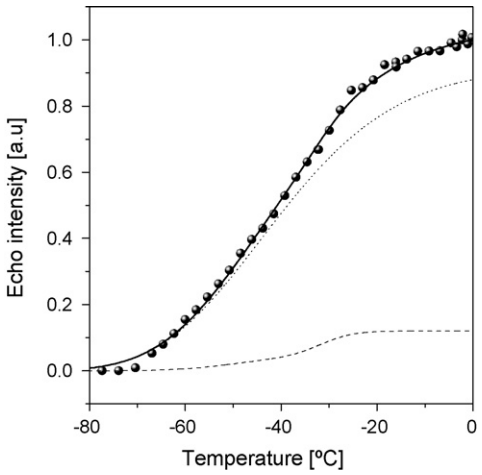

Fig. 8. Temperature dependence of the ^{1}H NMR echo intensity for an aqueous dispersion of colloidal silica coated by PDADMAC/(PSS/PAH)$_4$. Spheres: experimental data; dashed line: contribution of water in silica pores; dotted line: contribution of water in multilayer pores; solid line: fit of the experimental data with three modes [41].

A comparison of these pore sizes with cut-off values obtained by permeation experiments is instructive. Jin et al. [42] as well as Liu and Bruening [43] investigated the size-dependent transport of small molecules through PSS/PAH membranes. Their estimated cut-off sizes were 0.7 nm and about 1 nm, respectively. The agreement between this method and cryoporometry is remarkable, since both methods monitor porosity in completely different ways. While pore sizes from cryoporometry represent an average over all water-filled voids in the film, for permeation only paths which are interconnecting sufficiently large pores are relevant. The agreement can be understood as indication of a very homogeneous nanostructure of polyelectrolyte multilayers.

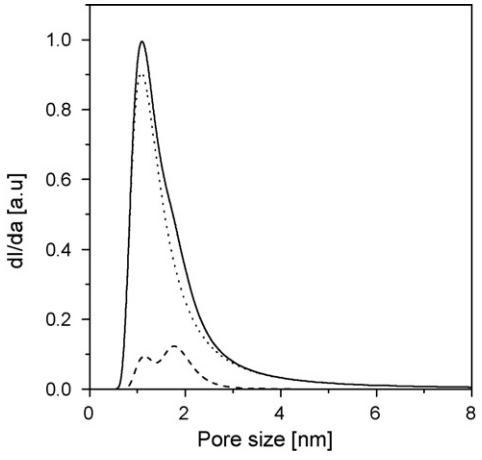

Fig. 9. Pore size distribution for colloidal silica coated by PDADMAC/(PSS/PAH)$_4$ as extracted from Fig. 8. Dashed line: contribution of water in silica pores; dotted line: contribution of water in multilayer pores; solid line: total distribution [41].

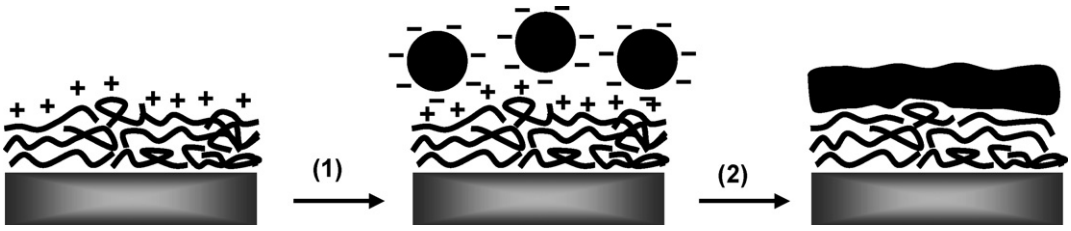

Scheme 1. Description of the two-step process generating an impervious capping layer on a polyelectrolyte film: step 1, electrostatic adsorption of charged wax nanoparticles; step 2, subsequent fusion of the wax nanoparticles.

2.5. Controlling water uptake: PEM nano-waterproofing by wax particles

Since polyelectrolyte films are highly hydrophilic, they are sensitive to environmental conditions such as atmospheric humidity (see Section 2.1), high or low pH and high ionic strength [14,17,44–47]. This sensitive behavior may cause the denaturation or the destruction of the film at extreme conditions. The stability of PEMs in dependence on external parameters has been compared to the conditions for multilayer formation in solution [48,49].

Different routes have been explored to reduce the permeability of the films towards water or small polar molecules. They are essentially based on the deposition of a hydrophobic coating atop the self-assembly. For instance, poly(styrene) (PS) and Nafion layers were successfully adsorbed onto the films, presumably preventing penetration by water [50,51]. However, this requires the presence of an organic solvent for the deposition of the hydrophobic polymer. Charged nanoparticles were also adsorbed onto polyelectrolyte multilayers and subsequently hydrophobically modified to produce super hydrophobic surfaces [52,53]. In analogy with biological membranes, uniform lipid bilayers were also deposited on polyelectrolyte multilayers [54–59]. Even if these lipid bilayers were shown to efficiently prevent the diffusion of small molecules in the films, they suffer from mechanical instability under stress. Here, an alternative approach was explored, which consisted of the adsorption of charged wax nanoparticles atop the multilayers followed by the subsequent melting of the particles at the moderate temperature (Scheme 1) [20]. This two-step process which generates a hydrophobic capping layer, was tested on $(PAH/PSS)_n$ multilayers with a positively charged outer surface.

The deposition of negatively charged wax nanoparticles onto the polyelectrolyte multilayers was successfully achieved as evidenced by the inspection of the characteristics of the coated and uncoated films reported in Table 1. The immersion of the polyelectrolyte film in the wax suspension caused an increase of the film thickness, accompanied by a large increase of the water contact angle. Moreover, the inspection of the morphology of the wax-coated film by AFM revealed that the wax particles are randomly distributed over the surface [20].

The fusion of the wax nanoparticles into a continuous layer after annealing at 60 °C was also evidenced by the decrease of the average ellipsometric thickness of the wax-coated films upon annealing (Table 1).

The study of the swelling behavior of uncoated and wax-coated films was performed by neutron reflectivity (NR) in D_2O. Indeed, a direct view of the distribution of D_2O within the film can be obtained by this technique due to the sensitivity of NR to deuterium. The scattering length density profiles computed for films immersed in D_2O [20] were converted to D_2O depth profiles. Fig. 10 displays the results obtained for uncoated $(PAH/PSS)_{9.5}$ and wax-coated and annealed $(PAH/PSS)_{9.5}$/wax film. The D_2O profile determined for uncoated sample revealed a high penetration by water accompanied by an increase of the film thickness. In contrast, the amount of D_2O incorporated in the wax-covered and annealed film was much lower and strongly decreased with increasing proximity to the silica substrate.

These results demonstrate that the deposition of wax nanoparticles atop the polyelectrolyte multilayers, followed by the

Table 1
Characteristics of wax-coated and uncoated polyelectrolyte films before and after annealing at 60 °C

Sample	Before annealing		After annealing
	Thickness (nm)	Contact angle (°)	Thickness (nm)
$(PAH/PSS)_{7.5}$	24 ± 1	46 ± 3	24 ± 1
$(PAH/PSS)_{7.5}$/wax	45 ± 3	100 ± 4	35 ± 2

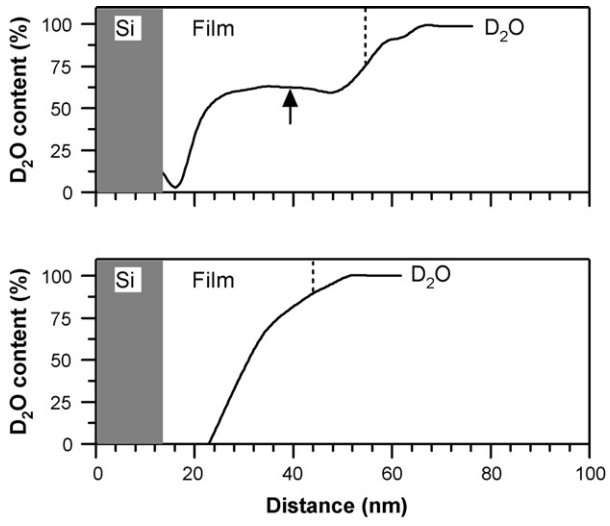

Fig. 10. Distribution of D_2O in polyelectrolyte multilayers as determined by neutron reflectivity measurements: $(PAH/PSS)_{9.5}$ (top) and $(PAH/PSS)_{9.5}$/wax annealed at 60 °C (bottom). The vertical arrow indicates the thickness of $(PAH/PSS)_{9.5}$ film measured in the dry state. The dashed lines indicate the average thickness of the films in D_2O. The D_2O depth profiles were computed from scattering length density (SLD) profiles [20].

subsequent fusion of the nanoparticles, generates an effective barrier layer which prevents penetration by water. This method should be promising to preserve the performance of multilayer films against environment.

3. Material properties of polyelectrolyte multilayers

3.1. Dielectric properties

Dielectric properties of PEM have so far been characterized by impedance and dielectric spectroscopy [60], and by determining internal polarity by fluorescent probes [61]. A novel way to monitor dielectric properties of PEM was recently demonstrated by a silicon-on-insulator (SOI)-based thin film resistor. Differently charged polyelectrolytes adsorbing to the sensor surface resulted in defined potential shifts. The response of the device can be modeled assuming electrostatic screening of polyelectrolyte charges by mobile ions within the PEMs. The screening length κ^{-1} inside the PEMs was found to be increased compared to the value corresponding to the bulk solution. The partitioning of mobile ions between the bulk phase and the polyelectrolyte film can be employed to calculate the dielectric constant of the PEMs and the concentration of mobile charges. For different polycations, significant differences in the dielectric constants of the polyelectrolyte films and in the concentration of mobile ions have been observed.

Field effect devices allow the determination of the surface potential at the sensor/electrolyte interface. However, this technique is best suited to quantify variations of the surface potential rather than absolute values, as most times important parameters such as contact potential, number of surface sites or quality of the oxide are not accessible. In contrast, in electrokinetic studies absolute results can be obtained. In these measurements, the zeta-potential at a shear plane outside the outer Helmholtz plane is determined with respect to the outer solution bulk value. Thus, for PEM the zeta-potential is measured at the side where new layers are adsorbed, whereas field effect devices measure the surface potential at the substrate/polyelectrolyte interface. Therefore, the latter are strongly dependent on screening effects within the polyelectrolyte films, which are not accessible by zeta-potential measurements. A direct comparison of zeta-potential measurements with surface potential measurements is of extreme difficulty as different boundary conditions apply for either experiment. In the case of zeta-potential measurements the boundary conditions for the solution of the Poisson–Boltzmann equation are given by the surface charge of the substrate and total charge neutrality which immediately leads to alternating zeta-potentials independent of the number of layers assuming the same absolute charge densities for adjacent PE layers. In contrast, in our system the boundary conditions are given by a constant reference voltage. Combined measurements of surface potential and zeta-potential have shown that even for uncoated substrates variations of the surface potential and the zeta-potential can differ by an order of magnitude [62] as the zeta-potential is measured *outside* the outer Helmholtz plane at a distance of a few Ångströms from the surface. For both electrokinetic and surface potential measurements, care must be taken to control the pH as well as the type and concentration of ions in the buffer solution. In addition, surface properties such as the density of surface sites that can be protonated or deprotonated have an influence on the measured potentials. In the case of field effect devices the surface site density strongly influences the charge sensitivity of the sensor because any change of surface charge caused by adsorbed molecules can partially be compensated by protonation or deprotonation. These effects can alter the response to charge adsorption. However, relative measurements, such as the dependence of the charge sensitivity with increasing distance to the surface, are not affected [63].

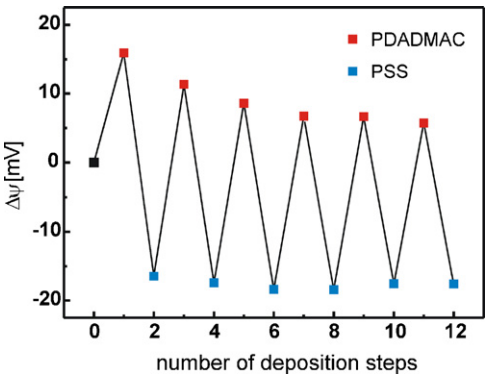

Fig. 11. Change in surface potential $\Delta\psi$ caused by the adsorption of polyelectrolyte layers against number of deposition steps. The buildup of multilayers consisting of PDADMAC and PSS is shown. The calibration measurement allows the calculation of $\Delta\psi$ from the change in sheet resistance shown in Fig. 12.

A silicon-on-insulator (SOI)-based field effect device can be used to monitor in real time the buildup of PEM. A theoretical description has been introduced to relate the response of such a device to the properties of the PEM [64]. The model allows the determination of the dielectric constant and the concentration of mobile ions within the films.

The sensor chips were fabricated from commercially available silicon-on-insulator (SOI) wafers as described in [65,66]. The sheet resistance of the device was monitored continuously during the multilayer deposition. The deposition of alternately charged polyelectrolytes resulted in defined shifts of the sheet resistance. First, the sensor was equilibrated with pure buffer solution. Next, a solution containing the polycation was injected, such that the positively charged polymers bind to the negatively charged silicon oxide surface decreasing the sheet resistance. The chip was rinsed with buffer solution and the anionic PSS was injected. The adsorption of the negatively charged molecules increased the sheet resistance. The system was rinsed with buffer and the deposition cycle could be repeated. Fig. 11 shows the corresponding change in surface potential $\Delta\psi$ for the buildup of PDADMAC/PSS multilayers.

$\Delta\psi$ was determined from the change in sheet resistance using the calibration measurement. The change of the surface potential $\Delta\psi$ between adjacent depositions of polycation and polyanion was plotted against the number of deposition steps in Fig. 12. Here, $\Delta\psi$ is shown for two different polycations PDADMAC and PAH in combination with PSS adsorbed from buffer containing 50 mM NaCl. $\Delta\psi$ decreases with increasing layer number

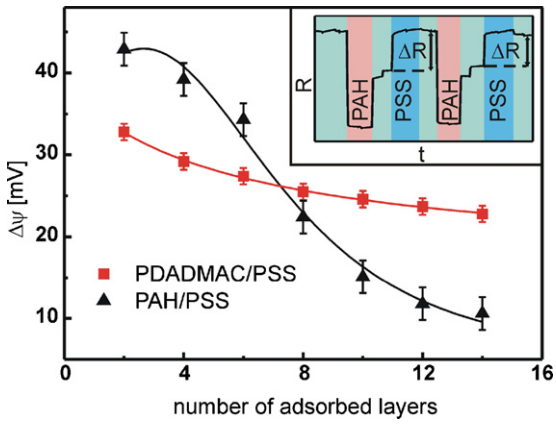

Fig. 12. Amplitude of the surface potential oscillations during multilayer buildup as a function of the number of adsorbed layers. The change of surface potential between adjacent depositions is calculated from the change of sheet resistance ΔR as indicated in the inset for the deposition of PAH/PSS films. Values for the screening length inside the polyelectrolyte films are obtained from a fit (solid curves).

and thus with increasing distance from the sensor surface which can be explained in terms of Debye screening of polyelectrolyte charges by mobile ions. The screening length κ^{-1} inside the PEMs was obtained from a fit of $\Delta\psi$ as a function of the number of layer. For both systems, κ^{-1} was increased compared to the values corresponding to the bulk solution. κ^{-1} was determined by the concentration of mobile ions and by the dielectric constant ε. The partitioning of mobile ions between the bulk phase and the polyelectrolyte film can be employed to calculate ε and the concentration of mobile charges from κ^{-1} [64]. Interestingly, the signal decrease is much faster for the PAH/PSS ($\kappa^{-1} = 6$ nm) system as compared to PDADMAC/PSS ($\kappa^{-1} > 33$ nm) [67]. These values for κ^{-1} correspond to a dielectric constant $\varepsilon = 30$ for PAH/PSS and $\varepsilon < 19$ for PDADMAC/PSS. Concentrations of mobile ions are in the order of 1 mM for PAH/PSS and <0.02 mM for PDADMAC/PSS. The different values found can be interpreted in terms of a different chemical structure of the polycation backbone. The deposition of PAH/PSS films has also been studied from buffer solution containing 500 mM NaCl [64]. Here, $\varepsilon = 21$ and a concentration of mobile ions of 0.6 mM has been found. Differences in the dielectric constant of PEM deposited from solutions of different ionic strength can be either explained in terms of a different water content of the films or by a different fraction of immobilized to free water as oriented water molecules show a decreased dielectric constant.

In comparison to the ion content extracted from structural methods, which amounts to about 0.1 M [19], thus, the content of mobile ionsin PEMs is far lower, and the method described here is unique in yielding concentrations of mobile ions.

3.2. *Permeability of exponentially growing polyelectrolyte multilayers towards multivalent small ions*

Polyelectrolyte multilayers can be used as ion separation membranes [68,69] and for this aim one has to understand and to engineer their permeation behavior towards species of varying charge and size. Most previous studies described the permeation behavior of linearly growing films such as PSS/PAH [70] or PSS/PDADMAC [71,72]. As a general trend, it was found that such films display small permeability towards multivalent ions (like hexacyanoferrate (II), osmium bipyridine and ruthenium hexaamine) as long as a minimum number of pairs of layers was deposited atop the working electrode. This critical number of layer pairs, usually between 3 and 5, depends on the chosen polyelectrolyte combination as well as on the film deposition conditions. The permeability of these kinds of compact multilayers, in which the internal charge compensation is mostly of "intrinsic" nature is small. By "intrinsic" charge compensation it is meant that the amount of charges provided by the polycation matches closely the amount of charges provided by the polyanion in the bulk of the film [73]. The permeability could be increased by performing the film buildup from solutions of higher ionic strength [72]. This behavior was rationalized by means of an ion doping model: sites for multivalent ions can be created when the film was previously swollen by an increase in ionic strength [74]. The fact that the PSS/PDADMAC combinations of polyelectrolytes may lead to strongly impermeable films allows to produce anticorrosive coatings [75]. However, it has to be noticed that the films made from PSS and PAH are highly permeable to protons owing to their small size and hydration [40].

Some polyelectrolyte multilayer films whose permeation selectivity can be pH switched for anions or cations have also been produced and characterized [76,77].

In comparison to the number of studies performed with synthetic polyelectrolytes, whose layer-by-layer self-assembly most often leads to linear film growth (at small to intermediate ionic strengths), up to now only a small amount of research has been reported which describes the permeability of exponentially growing films to multivalent ions [77–79].

Cyclic voltammetry was used to acquire knowledge about the internal charge distribution and the permeability of exponentially growing polyelectrolyte multilayers [80,81] with respect to multivalent (positively and negatively) charged redox probes. It is the aim of this part of the review to summarize recent findings in this field and to estimate a reasonable value of the Donnan potential inside PEI–(PGA–PAH)$_n$ multilayer films [82]. The very peculiar behavior displayed by the PEI–(HA–PLL)$_n$ films (HA: hyaluronan) will also be described [83]. Finally some perspectives will be given concerning some applications of these films acting as selective ion traps.

The permeability of PEI–(PGA–PAH)$_{10}$, PEI–(PGA–PAH)$_{10}$–PGA (hence films differing in their nature only by their last deposited layer), PEI–(HA–PLL)$_7$ and PEI–(HA–PLL)$_7$–HA films was investigated by combining cyclic voltammetry on gold electrodes and Fourier transformed infrared spectroscopy in the totally attenuated reflection mode (ATR-FTIR). The full experimental details can be found in Refs. [82,83].

As a first result it was found that PEI–(PGA–PAH)$_{10}$ or PEI–(PGA–PAH)$_{10}$–PGA multilayer films, whose thickness was close to 1 μm [81], were highly permeable to the tetravalent $Fe(CN)_6^{4-}$ anions and that the permeation kinetics needed over about 2–3 h to reach a steady-state (Fig. 13). It is also noteworthy

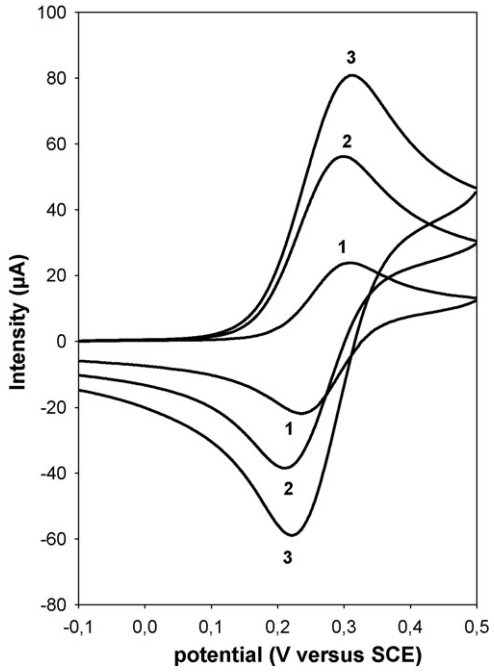

Fig. 13. Time evolution of the cyclic voltamograms (performed at a scan rate of 200 mV/s) on a gold electrode covered with a PEI–$(PGA–PAH)_{10}$ film and put in contact (at time $t = 0$) with a Tris–NaCl buffer containing 1 mM of $Fe(CN)_6^{4-}$ [82]. Curve 1 was taken immediately after the electrode immersion into the solution, curves 2 and 3 were acquired after 20 and 240 min of incubation, respectively.

that the cyclic voltamograms were characteristic of a reversible process with a spacing between the oxidation and reduction peaks close to 70 mV (the theoretical value for a one electron process at 298 K is 59 mV). This result is totally different from that obtained on PEI–$(PSS–PAH)_{10}$ or PEI–$(PSS–PAH)_{10}$–PSS films whose buildup was performed under the same conditions: in agreement with literature data these films were totally impermeable to hexacyanoferrate (II) [70]. In addition, for the $(PGA–PAH)_n$ films, the steady-state values of the oxidation and reduction peak currents were only slightly sensitive to the nature of the last deposited polyelectrolyte: in the case were the hexacyanoferrate (II) containing buffer was put in contact with the PAH ending film, which was expected to act as a trap for these anions, the oxidation and reduction currents were only about 20% higher than for PGA ending films.

This finding pointed to the fact that the bulk of the film acts as a trap for the negatively charged hexacyanoferrate (II) ions. This might well be the consequence of an "extrinsic" internal charge compensation with an excess positive charge afforded by the amino groups of PAH (these charges then being compensated not only by carboxylate groups from PGA but also by the Cl^- ions present in the Tris–NaCl buffer). To validate this assumption, permeation experiments were performed by immersing the same films into Tris–NaCl buffer containing the positively charged ruthenium hexaamine. Indeed, as expected, the cyclic voltamograms were purely capacitive curves with no detectable oxidation/reduction peaks.

Hence these PGA–PAH multilayer films buildup at pH 7.4 must display a positive Donnan potential. These findings are in total agreement with those of Noguchi and Anzai in the case of (alginic acid–PAH) containing multilayer films [79].

By rinsing the hexacyanoferrate (II) saturated films with pure Tris–NaCl buffer it was found that the amount of released species was always smaller than 15%. Cyclic voltammetry experiments on these films were then performed at different scan rates: it was found that the peak currents for both the oxidation and reduction processes varied linearly with the potential scan rate: this is typical for a thin film behavior. Moreover, at small scanning rates the oxidation and reduction peaks became symmetric: integration of the area under each of this peak yielded the a of charges of incorporated hexacyanoferrate (II) species which is equal to $(3.0 \pm 0.4) \times 10^{-4}$ C. Knowing the area of the electrode and the film thickness it was possible to estimate the concentration of the electroactive species inside the film, which resulted in (0.90 ± 0.50) mol/L. This concentration is about three orders of magnitude higher than in the bulk of the Tris–NaCl buffer containing 1 mM of hexacyanoferrate (II). Assuming equilibrium between the electroactive species in bulk solution and in the film, an estimate of the Donnan potential ϕ_D of the film was obtained, using the concentrations c_1 and c_2 of $Fe(CN)_6^{4-}$ in the film and in solution, respectively, and employing the Boltzmann relation [70]:

$$\frac{c_1}{c_2} = \exp\frac{4F\phi_D}{RT}$$

where T, F and R are the temperature, the Faraday constant and the ideal gas constant, respectively. The factor 4 is due to the four charges borne by the hexacyanoferrate (II) ions. The Donnan potential was thus estimated to be of the order of 44 ± 5 mV.

Owing to the very small and slow hexacyanoferrate (II) release in pure buffer, we investigated the effect of putting the $Fe(CN)_6^{4-}$ saturated multilayer in presence of either PGA or PAH solutions. When a PGA ending film was put in contact with a PGA solution at 1 mg/mL, both the oxidation and reduction currents decreased rapidly and were found to be identical to pure capacitive currents after about 30 min. When a PAH ending film was put in contact with a PAH solution the final result was the same as previously, though the release kinetics was slower: the oxidation and reduction currents totally vanished after about 60 min (Fig. 14).

This behavior cannot be attributed to a film dissolution process as was demonstrated by means of ATR-FTIR spectroscopy: when a film saturated with $Fe(CN)_6^{4-}$ was put in contact with a PGA solution, the absorbance due to the cyano groups of hexacyanoferrate (II) decreased, whereas the absorption due the amide I band, originating only from the PGA molecules, increased (Fig. 15). This demonstrates that the hexacyanoferrate (II) ions are exchanged by the PGA molecules diffusing into the film. Indeed, it was shown that the exponential growth of the PGA–PAH films is due to the diffusion of PGA into and out of the film when it is put in contact with PGA and PAH solutions, respectively [81].

The hexacyanoferrate (II) release from the PAH ending film when it is put in contact with a PAH solution cannot be explained by such an ion exchange mechanism, because PAH is not diffusing into such PGA–PAH multilayers in the time scale of about

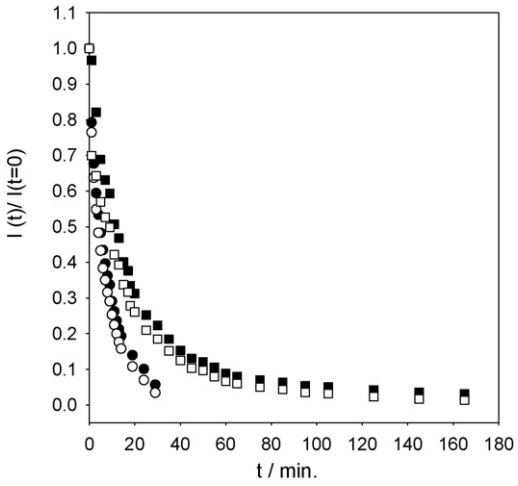

Fig. 14. Evolution of the peak current intensities with time when a PEI–(PGA–PAH)$_{10}$–PGA film saturated with hexacyanoferrate (II) is put in contact with a buffer solution containing PGA at 1 mg/mL (circles) and when a PEI–(PGA–PAH)$_{10}$ film is put in contact with a PAH (at 1 mg/mL) containing buffer (squares) [82]. The peak intensities are normalised to the peak current intensity at time $t = 0$, *i.e.* before the $Fe(CN)_6^{4-}$ containing films are put in contact with polyelectrolyte solutions. The closed and open symbols correspond to the oxidation and reduction currents, respectively.

1 h. Probably the PAH molecules in solution act as a trap able to slowly extract the hexacyanoferrate (II) anions out of the film.

Very interestingly, when the same kinds of experiments were performed on exponentially growing PEI–(HA–PLL)$_7$–HA films, quartz crystal microbalance measurements showed that hexacyanoferrate (II) ions induced an important, but not a quantitative, dissolution process of the multilayer film [83]. This behavior was attributed to the very weak cohesion of this kind of film: the interaction between the positively charged groups of PLL and hexacyanoferrate (II) should be stronger than the interactions between PLL and HA. An experimental evidence for that was provided in the following experiment: when, hexacyanoferrate (II) (carrying four elementary charges) is replaced by its oxidized form, $Fe(CN)_6^{3-}$, the HA–PLL film behaved like the PGA–PAH film did with respect to hexacyanoferrate (II). Indeed, the $Fe(CN)_6^{3-}$ ions were accumulating into the PEI–(HA–PLL)$_7$–HA films and were only removed from it when the film was put in contact with the diffusing polyelectrolyte, namely PLL [83]. Both of these studies [82,83] showed that it is possible to release a molecule embedded inside of the film by putting it in contact with a polyelectrolyte solution without a macroscopic change in pH. This is in contrast with most of the previous drug or dye release reported experiments from multilayer films which were realized upon a pH change [77] which has normally to be avoided for biological applications.

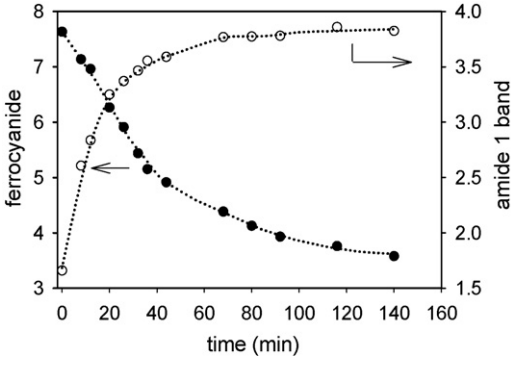

Fig. 15. Time evolution of the integrated absorbance due to hexacyanoferrate (II) (at 2033 cm^{-1}) and due to the amide I elongations of PGA (between 1600 and 1700 cm^{-1}) when a PEI–(PGA–PAH)$_{18}$ film saturated with hexacyanoferrate (II) is put in contact with a PGA solution at 1 mg/mL [82].

3.3. Influence of the sub-structure of PEM on their mechanical properties

The possibility to switch and/or tune the properties of PEM by external stimuli is of great interest to trigger the functional properties of the material such as the wettability, the (bio)adhesivity or the permeability [84]. Various biomacromolecules, such as carrageenans, are well known to show a pronounced change of their macromolecular conformation in aqueous solution with temperature, ionic strength or pH [85]. This conformational transition induces a strong variation of the stiffness and the effective volume of the macromolecular chains. This makes them promising candidates for formation of responsive materials. As a first step towards responsive materials, it was shown that variations of the polyelectrolyte chain conformation can significantly influence the internal structure as well as the mechanical behavior of the multilayer [86].

The multilayer assemblies were formed at pH 10 by alternatingly adsorbing a weak polycation (PAH) and two kinds of anionic sulfated polysaccharides (λ- and ι-carrageenan) which mainly differ by their conformation in solution (Fig. 16). Indeed, λ-carrageenan is known to present a random coil conformation in solution and cannot form gels [85], whereas ι-carrageenan

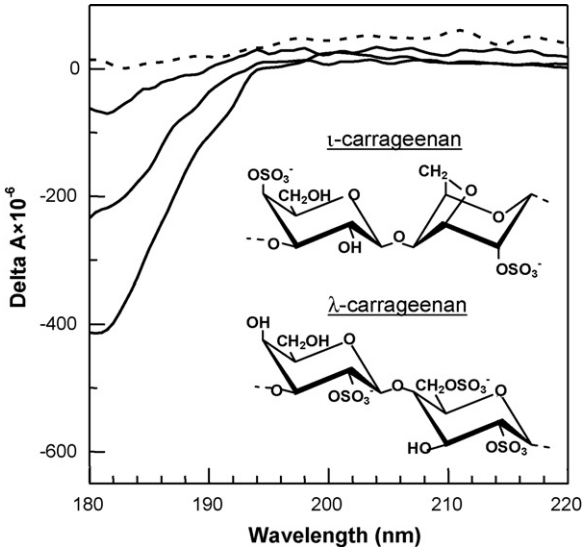

Fig. 16. Schematic representation of the disaccharide repeat units of ι- and λ-carrageenan and circular dichroism spectra of (PAH/λ-carr)$_{30}$ (dashed line) and (PAH/ι-carr)$_N$ (from top to bottom: $N = 8$, 15, and 30) (continuous lines) films measured at room temperature in dried state [86].

adopts a structured helical conformation at room temperature [85,87].

Circular dichroism (CD) measurements performed on $(PAH/\lambda\text{-carr})_N$ and $(PAH/\iota\text{-carr})_N$ films have confirmed that the conformation of the polysaccharides are kept during the formation of the multilayers (Fig. 16). Indeed, whereas no band was detected for optically non-active films containing λ-carrageenan, a clear decrease of the dichroic signal was observed at wavelengths below 195 nm for ι-carrageenan-based films. The observed decrease of the dichroic signal below 195 nm was in agreement with the presence of the negative band centered at 180 nm previously observed by others and due to the presence of the helical structure [88]. Furthermore, the CD spectra of $(PAH/\iota\text{-carr})_N$ multilayers of increasing thickness clearly showed that the higher the number of layers, the higher the intensity of the 180 nm band. From this, it was concluded that ι-carrageenan chains embedded into the film keep their structured helical conformation over the whole film thickness.

The influence of the polysaccharide conformation on the multilayer morphology was checked by performing AFM imaging measurements on 30-bilayer samples ended by a carrageenan layer [86]. Measurements were both carried out at room temperature on dried films and on films immersed in aqueous solution of pH 10. They revealed the presence of continuous films with very different morphologies depending on the carrageenan used. Indeed, adsorption of the flexible random coiled λ-carrageenan chains onto the multilayers resulted in the formation of rough multilayers (RMS roughness ∼110 nm in wet state) as frequently encountered when working with weakly charged polyelectrolytes such as PAH at pH 10 [89]. In contrast, the adsorption of stiff helices of ι-carrageenan led to the formation of a flat and well defined surface (RMS roughness ∼30 nm in wet state).

The mechanical behavior of the multilayer films was studied by the nano-indentation of an AFM tip into $(PAH/\lambda\text{-carr})_{30}$ and $(PAH/\iota\text{-carr})_{30}$ hydrated films at pH 10 [86,90,91]. The Young's modulus values were thus calculated from fitting the force versus deformation curves upon approach. Different models were used in order to investigate the influence of the thickness of the multilayer onto the elastic response of the material [92,93]. Compared to the Hertz model, the use of the thickness dependent models did not lead to significant improvements of the fit [86]. Therefore, the Hertz model was systematically used to analyze the data (Fig. 17). The relationship with the Young's modulus (E) is $F = 4/3(1-\nu^2)ER^{1/2}\delta^{3/2}$, where F represents the applied force, ν the Poisson ratio, R the radius of the AFM tip and δ the indentation depth.

Considering the nature of the studied materials and since no independent measurement allowed the determination of the exact Poisson ratio, a value of 0.33 was chosen for ν [94]. The tip radius (R) estimated after the surface modification by blind reconstruction of the tip geometry [95] was 50 nm. To obtain reliable results, similar force versus deformation measurements were performed in 40 different areas of the sample. The average Young's moduli extracted from these samplings and determined according to the Hertz model were 35 ± 5 and 7.5 ± 2 MPa for films prepared with λ- and ι-carrageenan, respectively. By considering this range of modulus values, the conclusion was that these hydrated films are relatively soft materials, like a typical elastomeric material [90,96]. Moreover, the larger stiffness and the higher value of Young's modulus measured for (PAH/ι-carr) films could be explained by the presence of structured helices which contribute to reinforce the mechanical properties of the assembly.

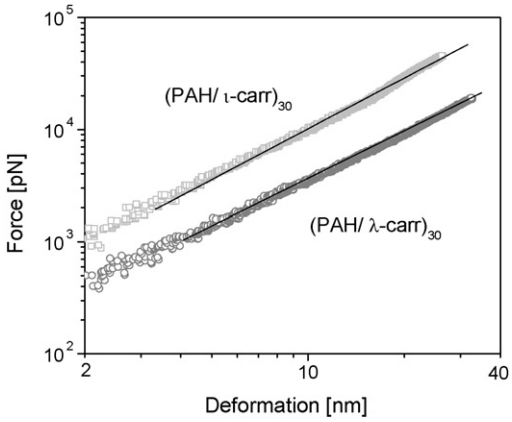

Fig. 17. Approaching force vs. deformation curves (in log–log) measured for $(PAH/\iota\text{-carr})_{30}$ and $(PAH/\lambda\text{-carr})_{30}$ films immersed in aqueous solution (pH 10). Full lines are Hertz fits to the data [86].

In conclusion, the formation of polyelectrolyte films based on a synthetic polycation, PAH and two different polysaccharides, ι- and λ-carrageenan, which mainly differ by their conformation, was monitored: the inspection of the morphology and the internal structure of the films clearly revealed that the helical conformation adopted by ι-carrageenan in solution was kept during the multilayer buildup. The presence of such ordered structures resulted in films with a higher thickness [86] and a higher Young's modulus compared to the unstructured λ-carrageenan-based ones. Evidence was provided that the characteristics and mechanical properties of multilayers strongly depend on the conformation of the polyelectrolyte chains used to prepare the films. The incorporation of responsive polyelectrolytes showing conformational transitions in multilayers should open new ways to tailor-responsive materials.

4. Conclusions

From a number of studies, the influence of the hydration water in PEM has become evident, as it plays an important role for the local structure. In addition, the degree of hydration controls film dynamics, since water as the solvent is sensitively tuning molecular interactions.

In the first decade of studies of PEM, the methodological approaches were dominated by classical structural techniques, for example reflectivity or QCM studies, which determine total layer thickness. These had mostly resulted in a simple picture of regular layer formation with linear or exponential growth.

Concerning detailed investigations, the present review documented several novel methodological approaches to study hydration water in PEMs, *i.e.* X-ray microscopy and NMR methods such as cryoporometry and solvent spin relaxation. These do

not only deliver novel types of information, such as pore sizes and water dynamics, but they are also important to close the gap between studies of planar PEMs and of colloidal systems, and to make studies of both types of films comparable. Another novel approach was to employ field effect devices for dielectric measurements.

Among other recent work, the experiments presented in this review lead to a far more complex view of the PEM system. Several aspects could be emphasized here: One is the complex influence that an adsorbed layer has on pre-deposited layers. This became obvious in the water content and dynamics, and furthermore had implications on the dielectric properties. Secondly, the relevance of polymer–solvent interactions is documented by the isotope effects of hydration water, which are larger than expected.

Further detail about the structure of water in the polymer network is provided by the discussion of the hydration kinetics in terms of voids filled with water, or the interpretation in terms of water pores, for which the size distribution can be analyzed. In this context, first models of the water distribution in PEMs are emerging and will surely become more detailed in the near future. They will have to be brought in connection to porosity and permeation studies, where most work has been done on ionic probes in PEM. These results are more complex to interpret, since the specific influence of electrostatic forces has to be considered, as demonstrated by the study of polyvalent ions in PEM presented here.

In addition to these microscopic questions of solvation and molecular interactions, the structure and dynamics of PEM on a longer length scale, *i.e.* the contour length of the chain, is relevant. This is demonstrated by the dependence of PEM mechanical properties on the polymer conformation, and furthermore by the heterogeneous structures formed by incorporation of wax particles.

Finally, an advanced understanding of PEM, in particular their dynamic properties, has to take into account the interplay of both long-range forces and the fine tuning of molecular forces within the stratified layers. This interplay of local and mesoscopic structure and dynamics makes PEMs very interesting and challenging materials.

Acknowledgement

The major part of the work reviewed in this article was performed within the German–French Collaborative Research Group ‘Complex Fluids: from 3 to 2 Dimensions’. This program is jointly funded by the Deutsche Forschungsgemeinschaft (DFG, Germany), Project nos. Ba 2029/4-3, Fi 235/14-1 to -4, Scho 636/3-1 to -2, and the Centre National de la Recherche Scientifique (CNRS, France).

References

[1] G. Decher, J.D. Hong, J. Schmitt, Buildup of ultrathin multilayer films by a self-assembly process. Part 3. Consecutively alternating adsorption of anionic and cationic polyelectrolytes on charged surfaces, Thin Solid Films 210 (1992) 831–835.

[2] E. Donath, G.B. Sukhorukov, F. Caruso, S.A. Davis, H. Möhwald, Novel hollow polymer shells by colloid-templated assembly of polyelectrolytes, Angew. Chem. Int. Ed. 37 (1998) 2202–2205.

[3] G.B. Sukhorukov, E. Donath, H. Lichtenfeld, E. Knippel, M. Knippel, A. Budde, H. Möhwald, Layer-by-layer self assembly of polyelectrolytes on colloidal particles, Colloid Surf. A 137 (1998) 253–266.

[4] G. Decher, Fuzzy nanoassemblies: toward layered polymeric multicomposites, Science 277 (1997) 1232–1237.

[5] P.T. Hammond, Recent explorations in electrostatic multilayer thin film assembly, Curr. Opin. Colloid Interf. Sci. 4 (1999) 430–442.

[6] P. Bertrand, A. Jonas, A. Laschewsky, R. Legras, Ultrathin polymer coatings by complexation of polyelectrolytes at interfaces: suitable materials, structure and properties, Macromol. Rapid Commun. 21 (2000) 319–348.

[7] Rv. Klitzing, R. Steitz, in: S.K. Triphaty, H.S. Nalva (Eds.), Handbook of Polyelectrolytes, American Scientific Publishers, 2002, pp. 313–334.

[8] M. Schönhoff, Self-assembled polyelectrolyte multilayers, Curr. Opin. Colloid Interf. Sci. 8 (2003) 86–95.

[9] M. Schönhoff, Layered polyelectrolyte complexes: physics of formation and molecular properties, J. Phys.-Condens. Matter 15 (2003) R1781–R1808.

[10] Rv. Klitzing, Internal structure of polyelectrolyte multilayer assemblies, Phys. Chem. Chem. Phys. 8 (2006) 5012–5033.

[11] A.A. Antipov, G.B. Sukhorukov, Polyelectrolyte multilayer capsules as vehicles with tunable permeability, Adv. Colloid Interf. Sci. 111 (2004) 49–61.

[12] G. Sukhorukov, A. Fery, H. Möhwald, Intelligent micro- and nanocapsules, Prog. Polym. Sci. 30 (2005) 885–897.

[13] Y. Lvov, G. Decher, H. Möhwald, Assembly, structural characterization, and thermal-behavior of layer-by-layer deposited ultrathin films of poly(vinyl sulfate) and poly(allylamine), Langmuir 9 (1993) 481–486.

[14] G.B. Sukhorukov, J. Schmitt, G. Decher, Reversible swelling of polyanion/polycation multilayer films in solutions of different ionic strength, Berichte Der Bunsen-Gesellschaft—Phys. Chem. Chem. Phys. 100 (1996) 948–953.

[15] M. Lösche, J. Schmitt, G. Decher, W.G. Bouwman, K. Kjaer, Detailed structure of molecularly thin polyelectrolyte multilayer films on solid substrates as revealed by neutron reflectometry, Macromolecules 31 (1998) 8893–8906.

[16] H. Ahrens, K. Büscher, D. Eck, S. Förster, C. Luap, G. Papastavrou, J. Schmitt, R. Steitz, C.A. Helm, Poly(styrene sulfonate) self-organization: electrostatic and secondary interactions, Macromol. Symp. 211 (2004) 93–105.

[17] R. Steitz, V. Leiner, R. Siebrecht, R. von Klitzing, Influence of the ionic strength on the structure of polyelectrolyte films at the solid/liquid interface, Colloid Surf. A 163 (2000) 63–70.

[18] T. Farhat, G. Yassin, S.T. Dubas, J.B. Schlenoff, Water and ion pairing in polyelectrolyte multilayers, Langmuir 15 (1999) 6621–6623.

[19] J.A. Jaber, J.B. Schlenoff, Counterions and water in polyelectrolyte multilayers: a tale of two polycations, Langmuir 23 (2007) 896–901.

[20] K. Glinel, M. Prevot, R. Krustev, G.B. Sukhorukov, A.M. Jonas, H. Möhwald, Control of the water permeability of polyelectrolyte multilayers by deposition of charged paraffin particles, Langmuir 20 (2004) 4898–4902.

[21] T.J. Halthur, U.M. Elofsson, Multilayers of charged polypeptides as studied by in situ ellipsometry and quartz crystal microbalance with dissipation, Langmuir 20 (2004) 1739–1745.

[22] T. Sasaki, Y. Ebina, T. Tanaka, M. Harada, M. Watanabe, G. Decher, Layer-by-layer assembly of titania nanosheet/polycation composite films, Chem. Mater. 13 (2001) 4661–4667.

[23] E.R. Kleinfeld, G.S. Ferguson, Rapid, reversible sorption of water from the vapor by a multilayered composite film: a nanostructured humidity sensor, Chem. Mater. 7 (1995) 2327–2331.

[24] Rv. Klitzing, J.E. Wong, S. Schemmel, R. Steitz, Exp. PHY-04-822, HMI, Berlin. Exp. PHY-04-822, HMI, Berlin, 2003.

[25] J.E. Wong, S. Schemmel, R. Steitz, Rv. Klitzing, Exp. PHY-04-964, 2004, HMI, Berlin. Exp. PHY-04-964, 2004, HMI, Berlin, 2004.

[26] J.E. Wong, F. Rehfeldt, P. Hanni, M. Tanaka, R.V. Klitzing, Swelling behavior of polyelectrolyte multilayers in saturated water vapor, Macromolecules 37 (2004) 7285–7289.
[27] P. Guttmann, B. Niemann, S. Rehbein, C. Knochel, D. Rudolph, G. Schmahl, The transmission X-ray microscope at BESSY II, J. Phys. IV 104 (2003) 85–90.
[28] K. Köhler, D.G. Shchukin, H. Möhwald, G.B. Sukhorukov, Thermal behavior of polyelectrolyte multilayer microcapsules. Part 1. The effect of odd and even layer number, J. Phys. Chem. B 109 (2005) 18250–18259.
[29] D. Yoo, S.S. Shiratori, M.F. Rubner, Controlling bilayer composition and surface wettability of sequentially adsorbed multilayers of weak polyelectrolytes, Macromolecules 31 (1998) 4309–4318.
[30] M. Müller, M. Brissova, T. Rieser, A.C. Powers, K. Lunkwitz, Deposition and properties of polyelectrolyte multilayers studied by ATR-FTIR spectroscopy, Mater. Sci. Eng. C 8–9 (1999) 163–169.
[31] A.F. Xie, S. Granick, Local electrostatics within a polyelectrolyte multilayer with embedded weak polyelectrolyte, Macromolecules 35 (2002) 1805–1813.
[32] M. Breit, M. Gao, G. von Plessen, U. Lemmer, J. Feldmann, S.T. Cundiff, Formation dynamics of layer-by-layer self-assembled films probed by second harmonic generation, J. Chem. Phys. 117 (2002) 3956–3960.
[33] B. Schwarz, M. Schönhoff, Surface potential driven swelling of polyelectrolyte multilayers, Langmuir 18 (2002) 2964–2966.
[34] B. Schwarz, M. Schönhoff, A H-1 NMR relaxation study of hydration water in polyelectrolyte mono and multilayers adsorbed to colloidal particles, Colloid Surf. A 198 (2002) 293–304.
[35] M. McCormick, R.N. Smith, R. Graf, C.J. Barrett, L. Reven, H.W. Spiess, NMR studies of the effect of adsorbed water on polyelectrolyte multilayer films in the solid state, Macromolecules 36 (2003) 3616–3625.
[36] R.N. Smith, M. McCormick, C.J. Barrett, L. Reven, H.W. Spiess, NMR studies of PAH/PSS polyelectrolyte multilayers adsorbed onto silica, Macromolecules 37 (2004) 4830–4838.
[37] D. Carrière, R. Krastev, M. Schönhoff, Oscillations in solvent fraction of polyelectrolyte multilayers driven by the charge of the terminating layer, Langmuir 20 (2004) 11465–11472.
[38] Rv. Klitzing, H. Möhwald, A realistic diffusion model for ultrathin polyelectrolyte films, Macromolecules 29 (1996) 6901–6906.
[39] P. Nazaran, H. Möhwald, Rv. Klitzing, submitted for publication.
[40] Rv. Klitzing, MöhwaldF H., Proton concentration profile in ultrathin polyelectrolyte films, Langmuir 11 (1995) 3554–3559.
[41] F. Vaca Chavez, M. Schönhoff, Pore size distributions in polyelectrolyte multilayers determined by cryoporometry, J. Chem. Phys. 126 (2007) 104705.
[42] W.Q. Jin, A. Toutianoush, B. Tieke, Size- and charge-selective transport of aromatic compounds across polyelectrolyte multilayer membranes, Appl. Surf. Sci. 246 (2005) 444–450.
[43] X.Y. Liu, M.L. Bruening, Size-selective transport of uncharged solutes through multilayer polyelectrolyte membranes, Chem. Mater. 16 (2004) 351–357.
[44] R. Kügler, J. Schmitt, W. Knoll, The swelling behavior of polyelectrolyte multilayers in air of different relative humidity and in water, Macromol. Chem. Phys. 203 (2002) 413–419.
[45] S.T. Dubas, J.B. Schlenoff, Swelling and smoothing of polyelectrolyte multilayers by salt, Langmuir 17 (2001) 7725–7727.
[46] S.T. Dubas, J.B. Schlenoff, Polyelectrolyte multilayers containing a weak polyacid: construction and deconstruction, Macromolecules 34 (2001) 3736–3740.
[47] E. Kharlampieva, S.A. Sukhishvili, Ionization and pH stability of multilayers formed by self-assembly of weak polyelectrolytes, Langmuir 19 (2003) 1235–1243.
[48] V. Izumrudov, E. Kharlampieva, S.A. Sukhishvili, Salt-induced multilayer growth: correlation with phase separation in solution, Macromolecules 37 (2004) 8400–8406.
[49] S.A. Sukhishvili, E. Kharlampieva, V. Izumrudov, Where polyelectrolyte multilayers and polyelectrolyte complexes meet, Macromolecules 39 (2006) 8873–8881.
[50] S. Sangribsub, P. Tangboriboonrat, T. Pith, G. Decher, Hydrophobization of multilayered film containing layer-by-layer assembled nanoparticle by Nafion adsorption, Polym. Bull. 53 (2005) 425–434.
[51] J.H. Rouse, G.S. Ferguson, Stepwise incorporation of nonpolar polymers within polyelectrolyte multilayers, Langmuir 18 (2002) 7635–7640.
[52] F. Shi, Z.Q. Wang, X. Zhang, Combining a layer-by-layer assembling technique with electrochemical deposition of gold aggregates to mimic the legs of water striders, Adv. Mater. 17 (2005) 1005.
[53] L. Zhai, F.C. Cebeci, R.E. Cohen, M.F. Rubner, Stable superhydrophobic coatings from polyelectrolyte multilayers, Nano Lett. 4 (2004) 1349–1353.
[54] R. Georgieva, S. Moya, S. Leporatti, B. Neu, H. Bäumler, C. Reichle, E. Donath, H. Möhwald, Conductance and capacitance of polyelectrolyte and lipid–polyelectrolyte composite capsules as measured by electrorotation, Langmuir 16 (2000) 7075–7081.
[55] S. Moya, E. Donath, G.B. Sukhorukov, M. Auch, H. Bäumler, H. Lichtenfeld, H. Möhwald, Lipid coating on polyelectrolyte surface modified colloidal particles and polyelectrolyte capsules, Macromolecules 33 (2000) 4538–4544.
[56] R. Kügler, W. Knoll, Polyelectrolyte-supported lipid membranes, Bioelectrochemistry 56 (2002) 175–178.
[57] C. Delajon, T. Gutberlet, R. Steitz, H. Möhwald, R. Krastev, Formation of polyelectrolyte multilayer architectures with embedded DMPC studied in situ by neutron reflectometry, Langmuir 21 (2005) 8509–8514.
[58] L. Wang, M. Schönhoff, H. Möhwald, Swelling of polyelectrolyte multilayer-supported lipid layers. Part 1. Layer stability and lateral diffusion, J. Phys. Chem. B 108 (2004) 4767–4774.
[59] G. Krishna, T. Shutava, Y. Lvov, Lipid modified polyelectrolyte microcapsules with controlled diffusion, Chem. Commun. (2005) 2796–2798.
[60] M.F. Durstock, M.F. Rubner, Dielectric properties of polyelectrolyte multilayers, Langmuir 17 (2001) 7865–7872.
[61] C. Tedeschi, H. Möhwald, S. Kirstein, Polarity of layer-by-layer deposited polyelectrolyte films as determined by pyrene fluorescence, J. Am. Chem. Soc. 123 (2001) 954–960.
[62] L.J. Bousse, S. Mostarshed, D. Hafeman, Combined measurement of surface-potential and zeta potential at insulator electrolyte interfaces, Sens. Actuators B-Chem. 10 (1992) 67–71.
[63] S.Q. Lud, M.G. Nikolaides, I. Haase, M. Fischer, A.R. Bausch, Field effect of screened charges: electrical detection of peptides and proteins by a thin-film resistor, Chemphyschem 7 (2006) 379–384.
[64] P.A. Neff, A. Naji, C. Ecker, B. Nickel, R. Von Klitzing, A.R. Bausch, Electrical detection of self-assembled polyelectrolyte multilayers by a thin film resistor, Macromolecules 39 (2006) 463–466.
[65] M.G. Nikolaides, S. Rauschenbach, S. Luber, K. Buchholz, M. Tornow, G. Abstreiter, A.R. Bausch, Silicon-on-insulator based thin-film resistor for chemical and biological sensor applications, Chemphyschem 4 (2003) 1104–1106.
[66] M.G. Nikolaides, S. Rauschenbach, A.R. Bausch, Characterization of a silicon-on-insulator based thin film resistor in electrolyte solutions for sensor applications, J. Appl. Phys. 95 (2004) 3811–3815.
[67] P.A. Neff, B.K. Wunderlich, R. Von Klitzing, A.R. Bausch, Formation and dielectric properties of polyelectrolyte multilayers studied by a silicon-on-insulator based thin film resistor, Langmuir 23 (2007) 4048–4052.
[68] L. Krasemann, A. Toutianoush, B. Tieke, Self-assembled polyelectrolyte multilayer membranes with highly improved pervaporation separation of ethanol/water mixtures, J. Membr. Sci. 181 (2001) 221–228.
[69] A.M. Balachandra, J.H. Dai, M.L. Bruening, Enhancing the anion-transport selectivity of multilayer polyelectrolyte membranes by templating with Cu^{2+}, Macromolecules 35 (2002) 3171–3178.
[70] S. Han, B. Lindholm-Sethson, Electrochemistry at ultrathin polyelectrolyte films self-assembled at planar gold electrodes, Electrochim. Acta 45 (1999) 845–853.
[71] T.R. Farhat, J.B. Schlenoff, Ion transport and equilibria in polyelectrolyte multilayers, Langmuir 17 (2001) 1184–1192.
[72] V. Pardo-Yissar, E. Katz, O. Lioubashevski, I. Willner, Layered polyelectrolyte films on Au electrodes: characterization of electron-transfer features at the charged polymer interface and application for selective redox reactions, Langmuir 17 (2001) 1110–1118.

[73] J.B. Schlenoff, H. Ly, M. Li, Charge and mass balance in polyelectrolyte multilayers, J. Am. Chem. Soc. 120 (1998) 7626–7634.
[74] T.R. Farhat, J.B. Schlenoff, Doping-controlled ion diffusion in polyelectrolyte multilayers: mass transport in reluctant exchangers, J. Am. Chem. Soc. 125 (2003) 4627–4636.
[75] T.R. Farhat, J.B. Schlenoff, Corrosion control using polyelectrolyte multilayers, Electrochem. Solid State Lett. 5 (2002) B13–B15.
[76] Y.L. Liu, M.Q. Zhao, D.E. Bergbreiter, R.M. Crooks, pH-switchable, ultrathin permselective membranes prepared from multilayer polymer composites, J. Am. Chem. Soc. 119 (1997) 8720–8721.
[77] S.E. Burke, C.J. Barrett, pH-dependent loading and release behavior of small hydrophilic molecules in weak polyelectrolyte multilayer films, Macromolecules 37 (2004) 5375–5384.
[78] Y.F. Cheng, L. Murtomaki, R.M. Corn, Electrochemical characterization of the ultrathin polypeptide film/1,2-dichloroethane liquid vertical bar liquid interface, J. Electroanal. Chem. 483 (2000) 88–94.
[79] T. Noguchi, J. Anzai, Redox properties of the ferricyanide ion on electrodes coated with layer-by-layer thin films composed of polysaccharide and poly(allylamine), Langmuir 22 (2006) 2870–2875.
[80] C. Picart, J. Mutterer, L. Richert, Y. Luo, G.D. Prestwich, P. Schaaf, J.C. Voegel, P. Lavalle, Molecular basis for the explanation of the exponential growth of polyelectrolyte multilayers, Proc. Natl. Acad. Sci. U.S.A. 99 (2002) 12531–12535.
[81] F. Boulmedais, V. Ball, P. Schwinte, B. Frisch, P. Schaaf, J.C. Voegel, Buildup of exponentially growing multilayer polypeptide films with internal secondary structure, Langmuir 19 (2003) 440–445.
[82] E. Hübsch, G. Fleith, J. Fatisson, P. Labbe, J.C. Voegel, P. Schaaf, V. Ball, Multivalent ion/polyelectrolyte exchange processes in exponentially growing multilayers, Langmuir 21 (2005) 3664–3669.
[83] V. Ball, E. Hubsch, R. Schweiss, J.C. Voegel, P. Schaaf, W. Knoll, Interactions between multivalent ions and exponentially growing multilayers: dissolution and exchange processes, Langmuir 21 (2005) 8526–8531.
[84] A. Schneider, G. Francius, R. Obeid, P. Schwinte, J. Hemmerle, B. Frisch, P. Schaaf, J.-C. Voegel, B. Senger, C. Picart, Polyelectrolyte multilayers with a tunable young's modulus: influence of film stiffness on cell adhesion, Langmuir 22 (2006) 1193–1200.
[85] F. van de Velde, G.A. De Ruiter, Biopolymers—Polysaccharides II, Wiley–VCH Verlag GmbH, Weinheim, 2002.
[86] B. Schoeler, N. Delorme, I. Donch, G.B. Sukhorukov, A. Fery, K. Glinel, Multilayer films based on polysaccharides of different secondary structures: effects on film structure and mechanical properties, Biomacromolecules 7 (2006) 2065–2071.
[87] K. Bongaerts, S. Paoletti, B. Denef, K. Vanneste, F. Cuppo, H. Reynaers, Macromolecules 33 (2000) 8709.
[88] J.S. Balcerski, E.S. Pysh, G.C. Chen, J.T. Yang, J. Am. Chem. Soc. 97 (1975) 6274.
[89] J.-L. Menchaca, B. Jachimska, F. Cuisinier, E. Perez, Colloids Surf. A 222 (2003) 185.
[90] L. Richert, A.J. Engler, D.E. Discher, C. Picart, Elasticity of native and cross-linked polyelectrolyte multilayer films, Biomacromolecules 5 (2004) 1908–1916.
[91] O. Mermut, J. Lefebvre, D.G. Gray, C.J. Barrett, Structural and mechanical properties of polyelectrolyte multilayer films studied by AFM, Macromolecules 36 (2003) 8819–8824.
[92] B.B. Akhremitchev, G.C. Walker, Finite sample thickness effects on elasticity determination using atomic force microscopy, Langmuir 15 (1999) 5630–5634.
[93] V.V. Tsukruk, A. Sidorenko, V.V. Gorbunov, S.A. Chizhik, Surface nanomechanical properties of polymer nanocomposite layers, Langmuir 17 (2001) 6715–6719.
[94] R. Mueller, K. Kohler, R. Weinkamer, G. Sukhorukov, A. Fery, Melting of PDADMAC/PSS capsules investigated with AFM force spectroscopy, Macromolecules 38 (2005) 9766–9771.
[95] J.S. Villarrubia, Morphological estimation of tip geometry for scanned probe microscopy, Surf. Sci. 321 (1994) 287–300.
[96] J. Heuvingh, M. Zappa, A. Fery, Salt softening of polyelectrolyte multilayer capsules, Langmuir 21 (2005) 3165–3171.